Effects of operating and design parameters on PEFC cold start

Kazuya Tajiri [a], Yuichiro Tabuchi [a,b], Fumio Kagami [b], Shinichi Takahashi [b],
Koudai Yoshizawa [b], Chao-Yang Wang [a,*]

[a] *Electrochemical Engine Center (ECEC), and Department of Mechanical and Nuclear Engineering,
The Pennsylvania State University, University Park, PA 16802, USA*
[b] *Nissan Motor Co. Ltd., Nissan Research Center, Kanagawa 237-8523, Japan*

Abstract

During startup from subzero temperatures the water produced in a polymer electrolyte fuel cell (PEFC) forms ice/frost in the cathode catalyst layer (CL), blocking the oxygen transport and causing cell shutdown once all CL pores are plugged with ice. This paper describes an experimental study on the effects of operating and design parameters on PEFC cold-start capability. The amount of total product water in $mg\,cm^{-2}$ during startup is used as an index to quantify the cold-start capability. The newly developed isothermal cold-start protocol is used to explore the basic physics of cold start, and the effects of purge methods prior to cold start, startup temperature and current density, and the membrane thickness are shown. The experimental data also confirm the current density effect predicted earlier by a multiphase model of PEFC cold start.

© 2006 Elsevier B.V. All rights reserved.

Keywords: Polymer electrolyte fuel cells; Cold start; Ice formation; Catalyst layer; Membrane

1. Introduction

A great challenge exists with the startup of a fuel cell vehicle from a subzero environment. During the operation of polymer electrolyte fuel cells (PEFC) the oxygen reduction reaction in the cathode catalyst layer (CL) produces water. At normal operation temperature (∼80 °C) the water produced can be removed either in vapor or liquid via vapor phase diffusion or capillary driven liquid flow. However, at subzero temperatures, the water forms ice/frost, accumulating in the voids of the cathode CL. Once the open pores are filled completely with ice/frost, oxygen transport to the catalyst sites is blocked, and the fuel cell is shut down. Meanwhile, the oxygen reduction reaction (ORR) also produces heat that increases the temperature of the fuel cell. If the cell temperature can rise above the freezing point before the CL is filled with ice that leads to shut down, the cold start is said to

be successful. This work seeks to identify key operating and design parameters that increase the operational time before cell shutdown and ensure self cold start.

Despite the technological importance, the effect of subzero temperatures on a PEFC has been scarcely studied. McDonald et al. [1] and Cho et al. [2,3] studied the impact of thermal cycling between a subzero temperature and the normal operating temperature on fuel cell performance. McDonald et al. [1] found that no phase transition of water within the membrane and no CL degradation occur, for dry membrane-electrode assembly (MEA) subject to freeze/thaw cycling between −40 and 80 °C. Cho et al. [2,3] instead claimed that the performance of wet cells degrade after only a few cycles. Note that no electrochemical reaction takes place and therefore no net water is produced in these freeze/thaw studies.

PEFC cold start, where water is produced in the cathode CL, was investigated by Hishinuma's group [4,5], both experimentally and numerically. They concluded that a cell can successfully start up only at temperatures higher than −3 °C. Later, Oszcipok et al. [6,7] conducted potentiostatic discharge

---

cold start from a very dry initial condition within the cell, and developed the statistical relationship of cumulative charge transfer density with air flow rate during startup and with initial membrane water content prior to startup.

To elucidate the fundamental principles underlying PEFC cold start, a series of experimental and modeling studies were published by Wang's group [8–11]. Ge and Wang [8] used a transparent cell to visualize ice formation on the catalyst layer in an operating fuel cell, and showed that the freezing point depression in the CL pores is no larger than 3 °C. Therefore, for a practical fuel cell vehicle cold start that is typically from −20 °C or lower, the freezing point depression is inconsequential. Mao and Wang [9] delineated the governing physics of water and heat balance in PEFC cold start and presented an analytical model to forecast key parameters such as the initial membrane water content prior to cold start and thermal mass of bipolar plates. Mao et al. [10] further developed a multiphase, transient 3D model to simulate cold-start performance. The model accounted for ice/frost precipitation and growth in the cathode CL and gas diffusion layer (GDL), water transport at very low temperatures, heat transfer with phase transition, oxygen transport, electrochemical kinetics, and their mutual interactions. The 3D numerical model was extensively validated against the experimental data of Tajiri et al. [11] and those presented in this paper with good agreement. In addition to providing benchmark-quality data for model validation, the work of Tajiri et al. [11] described novel experimental procedures aimed at elucidating fundamentals of PEFC cold start. A method of equilibrium purge using partially humidified gas with well controlled relative humidity was introduced to effectively control initial water distribution inside a cell prior to cold start. Isothermal cold start, in which single cells with sufficiently large thermal mass are used to maintain the cell temperature at startup ambient temperature, was proposed to study intrinsic cold-start capability of a MEA. Also, the proton conductivity of membranes with low water content and at subzero temperatures was measured in situ for the first time. Finally, using the cumulative product water during startup as a quantitative measure of cold-start performance, Tajiri et al. [11] studied the effects of the membrane initial water content and the startup current density on cold start from −30 °C. This work revealed that the pore volume in the cathode CL is not fully utilized for water storage at high current densities.

Continuing the previous work of [11], we present in this paper comprehensive experimental data showing the effects of operating/design parameters on cold-start performance. The operating parameters examined here include the ambient startup temperature, the startup current density, and the initial water content of the membrane prior to cold start. Furthermore, two methods of gas purge used to create the initial condition for cold start are studied and compared. One is *equilibrium purge*, as described above, which can be used to accurately control the initial water condition in a cell and is particularly suited for fundamental research. The other is *dry purge* which uses dry air to purge a cell for short times (on the order of seconds) and mimics the practical purge process conducted on a fuel cell vehicle. With dry purge, the cell internal condition is less uniform and the cold-start performance differs from the equilibrium purge case.

Finally, as an important design parameter for a PEFC, the effect of membrane thickness is experimentally examined.

2. Experimental

2.1. Experimental setup

A laboratory-scale, single cell with 25 cm^2 active area is used for this study. In both anode and cathode sides of the cell, the straight, parallel channels of 54 mm length, 1 mm width, 0.6 mm depth with 1 mm-wide land form the flow field. The cell consists of two graphite bipolar plates, two current collectors of gold-plated stainless steel, two stainless steel end plates, and a membrane and electrode assembly (MEA). Because the heat capacity of the entire cell is large compared to the heat generation, the temperature rise of the cell is negligible and the cell temperature remains nearly constant at the ambient temperature throughout startup. Cold start under this thermal condition is called *temporally isothermal cold start*, an experimental protocol enabling the fundamental understanding of PEFC cold start, as the cold-start performance becomes independent of cell fixtures and depends solely on the intrinsic properties of the MEA. In addition, isothermal cold start provides the most conservative scenario for evaluation of the cold-start capability.

The MEAs used in this study are commercially available, with 0.4 mg cm^{-2} Pt loading on both anode and cathode (Japan Gore-Tex Inc.). The membrane thickness is 30 μm, unless otherwise noted, and Toray carbon papers with microporous layer are used as gas diffusion layer (GDL).

The fuel cell operation above freezing was controlled and tested using an Arbin fuel cell testing system (Arbin Instruments, College Station, TX). To cool down the cell and to generate subzero ambient temperatures for cold-start experiments, we used a Tenney environmental chamber (model T10C, Lunaire Limited, Williamsport, PA). During subzero startup the flow rates were controlled using float type flow meters directly connected to the gas cylinders in order to assure no water entered the cell. Throughout each cold-start experiment the high-frequency resistance (HFR) of the cell was measured with a Tsuruga milliohm meter (Model 3566, Osaka, Japan). More details on the experimental setup can be found in Tajiri et al. [11].

2.2. Equilibrium purge

Equilibrium purge prior to cold start allows accurate control of the initial water condition inside a cell. The experimental procedure of cold start with equilibrium purge consists of the following four steps: (1) initial conditioning, (2) equilibrium purge, (3) cool down, and (4) start up. The experimental conditions are summarized in Table 1. In the first step, the cell is conditioned at the discharge current density of 500 mA cm^{-2} for 30 min at 30 °C. The gases supplied to the cell in this stage are 1.57 L min^{-1} of H$_2$ and 4.48 L min^{-1} of air for anode and cathode, respectively. Both gases are fully humidified at 30 °C. In the second step, the cell is purged with 1 L min^{-1} of partially humidified N$_2$ with known relative humidity (RH) for more than 2 h. In this step all liquid water in the pores of the CL and GDL as well

Table 1
Experimental conditions for two purge modes

	Equilibrium purge	Dry purge
Purge cell temperature	30–60 °C	55 °C
Purge gas dew point	30 °C	Dry
Anode purge gas flow rate	1 L min^{-1}	2 L min^{-1}
Cathode purge gas flow rate	1 L min^{-1}	4.48 L min^{-1}
Purge duration	>2 h	15–90 s
Cold start current density	40 mA cm^{-2} with initial ramp of 0.5 mA cm^{-2} s^{-1}	100 mA cm^{-2}
Controlling parameter	Purge cell temperature (purge gas relative humidity)	Purge duration

as in gas channels is removed, and the membrane is equilibrated with the purge gas RH. By changing the cell temperature while fixing the gas dew point at 30 °C, the water activity with which the membrane is equilibrated is varied. At the end of step (2), the membrane water content is determined according to Springer's water uptake curve [12]

$$\lambda = 0.043 + 17.81a - 39.85a^2 + 36.0a^3 \tag{1}$$

where λ is membrane water content and a is water activity of the purge gas.

In the third step the cell is placed in the environmental chamber and cooled down to a prescribed startup temperature. During the cool down, the gas channels of the cell are closed at both the inlet and outlet such that the water content in the membrane does not change. Once the cell temperature reaches the specified temperature, the cell is left at that temperature for more than 1 h before proceeding to step (4) in order to assure the cell temperature is uniform throughout. In the final step (cell startup), the reactant gases start to flow and the open-circuit voltage rises, at which point the discharge operation begins with the initial current ramp of 0.5 mA cm^{-2} s^{-1} for 80 s and then the current density is kept constant at 40 mA cm^{-2} until the cell voltage drops below the cut-off voltage of 0.3 V. This current density profile is displayed in Fig. 1.
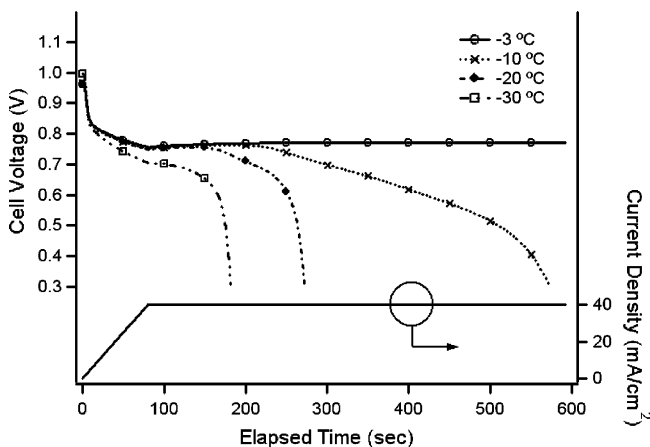
2.3. Dry purge

The second purge method, dry purge, was designed to simulate the realistic operation of a fuel cell vehicle. Similarly, a dry purge cold-start experiment consists of four steps: (1) the cell is operated with 500 mA cm^{-2} discharge current density for 15 min with both fully humidified 1.57 L min^{-1} H$_2$ and 4.48 L min^{-1} air at 55 °C; (2) the cell is purged at 55 °C with 2 and 4.48 L min^{-1} of dry N$_2$ for anode and cathode, respectively, and the dry purge duration is varied from 15 to 90 s as one of the operating parameters for study; (3) the cell is cooled down in the environmental chamber, in the same manner as in the equilibrium purge case, and the membrane water content is estimated by measuring the cell HFR at 10 °C during cool down via the proton conductivity and membrane water content relationship; and (4) a current density of 100 mA cm^{-2} is applied for cold start. Each experiment is terminated when the cell voltage drops to the cut-off voltage of 0.3 V.

3. Results and discussion

3.1. Effect of startup temperature after equilibrium purge

The effect of the startup temperature was studied by starting the cell at ambient temperatures of −3, −10, −20, and −30 °C. The initial water content in the membrane prior to cold start was fixed at $\lambda_i = 6.2$ for all startup temperatures. Fig. 1 shows the time evolution of current density and cell voltage during each startup. It can be seen that as the startup temperature increases, the fuel cell can operate much longer. At −3 °C the cell shows no significant voltage drop-down and is able to operate indefinitely.

In these startup experiments the initial current linear scan (0.5 mA cm^{-2} sec^{-1}, 0–80 s) can be viewed as a fast-scan polarization curve. The iR-free voltage during the initial current ramp is plotted with the current density in the logarithmic scale in Fig. 2 for four startup temperatures. Two remarkable features can be observed in Fig. 2. First, the lower the startup temperature, the lower the iR-free voltage becomes. This is mainly because
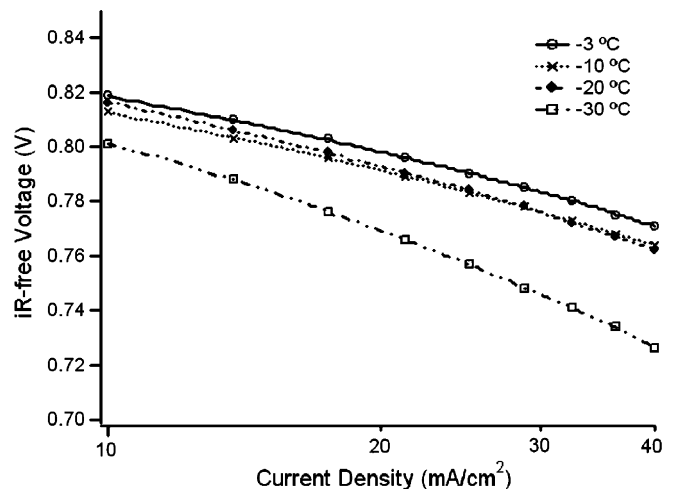

Fig. 1. Time evolution of current density and cell voltage at various startup temperatures after equilibrium purge ($\lambda_i = 6.2$).

Fig. 2. Current–voltage relations during linear current ramp at various startup temperatures after equilibrium purge ($\lambda_i = 6.2$).

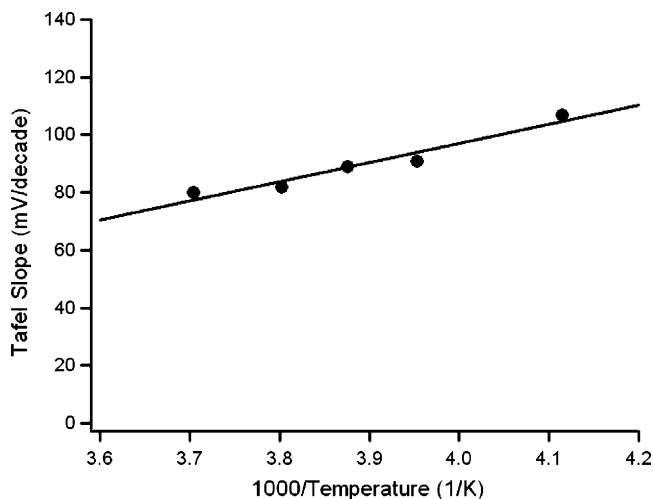Fig. 3. Effect of startup temperature on Tafel slope of oxygen reduction reaction ($\lambda_i = 6.2$).

Fig. 5. Relation between product water and membrane water uptake potential for the startup from -20 and $-30\,°C$ after equilibrium purge.

of slow ORR kinetics at low temperatures. Second, the slope of the lines (i.e. the Tafel slope of ORR) increases as the startup temperature decreases. The change of Tafel slope with temperature is plotted in Fig. 3. Note that the V-I curve for -30 °C in Fig. 2 bends downward, indicating the onset of the mass transport loss around 25 mA cm^{-2}. Therefore, in the $-30\,°C$ case, only the *I–V* data between 10 and 25 mA cm^{-2} were taken to calculate the Tafel slope in Fig. 3. Fig. 3 clearly shows that the Tafel slope increases from typically ~ 66 mV decade^{-1} under room temperature to ~ 105 mV decade^{-1} at $-30\,°C$.

Following Tajiri et al. [11], we use the cumulative product water till cell shutdown to quantify the cold-start performance. Fig. 4 depicts a strongly nonlinear relationship between the product water and the startup temperature. Primary reasons for large product water at high temperatures include the high proton conductivity, large water diffusivity in the membrane, facile ORR kinetics, and high saturation vapor pressure.

Since, as mentioned earlier, at $-3\,°C$ the cell can operate indefinitely at steady state, how is the water production rate of
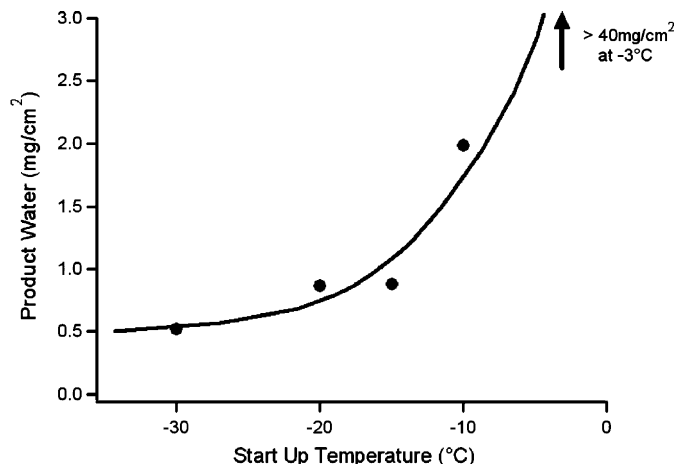

Fig. 4. Relation between product water and startup temperature under equilibrium purge ($\lambda_i = 6.2$) and current density of 40 mA cm^{-2}.

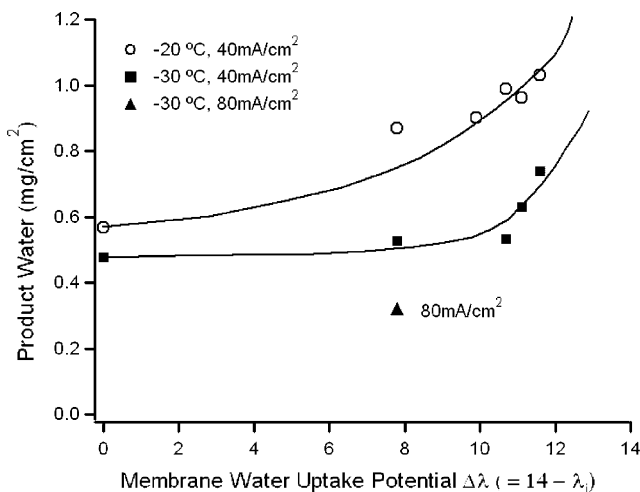0.0037 mg cm^{-2} sec^{-1} balanced by the water removal rate from the cathode CL? Assuming the exhaust gases from the cell are fully saturated with water vapor at the cell temperature of $-3\,°C$, 0.0012 mg cm^{-2} s^{-1} of water vapor can be removed from the cell, which is only 30% of the production rate. Therefore, to achieve steady state operation at $-3\,°C$, 0.0025 mg cm^{-2} s^{-1} of water must be removed from the cathode CL either in liquid or vapor. Indeed, Ge and Wang [8] observed that liquid water emerges from the CL surface at the cell plate temperature of $-3\,°C$, implying that the CL temperature is slightly higher than the ambient temperature because of the thermal gradient in GDL resulting from heat generation. Thus, it is likely that the water produced in the cathode CL is transported to the GDL in liquid phase by capillary forces and may freeze in the GDL pores or be further transported to the gas channels.

In Fig. 5 the product water is plotted against the membrane water uptake potential $\Delta\lambda$ for two startup temperatures, -20 and $-30\,°C$. The membrane water uptake potential $\Delta\lambda$ is defined as $\Delta\lambda = 14-\lambda_i$, where 14 denotes the water content for saturated Nafion membranes and λ_i is the initial membrane water content prior to the startup as controlled by changing the purge gas RH. As $\Delta\lambda$ increases, that is, when the initial membrane is dry, the product water during cold start increases, because more water from the CL can be absorbed and stored in the membrane. As indicated in [11], when $\Delta\lambda$ approaches zero (i.e. the initial membrane prior to cold start is fully hydrated), no water can be transported into the membrane and therefore the product water measured reflects the storage capacity in the cathode CL under very low temperatures such as $-20\,°C$. As seen from Fig. 5, this storage capacity amounts to ~ 0.5 mg cm^{-2}, which is in excellent agreement with the value estimated by Ge and Wang [8] based on the open pore volume of the cathode CL. When $\Delta\lambda > 0$, the product water can either accumulate in the cathode CL or transport into a partially hydrated membrane, thereby making the cumulative product water higher. At low temperatures such as -20 or $-30\,°C$, no water can transport from the CL into the GDL, either in the liquid or vapor phase. The liquid phase transport is ruled out according to the recent visualization study [8],
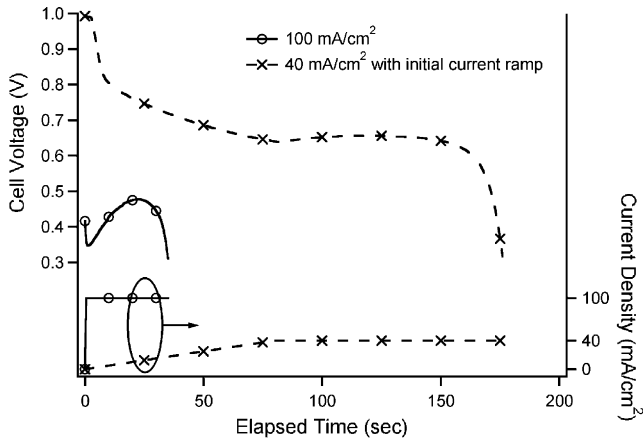
Fig. 6. Time evolution of current density and cell voltage during startup from $-30\,^\circ\text{C}$ with different current profiles ($\lambda_\text{i} = 1.9$).

Fig. 7. IR-free voltage change with cumulative product water during startup from $-30\,^\circ\text{C}$ with different current profiles ($\lambda_\text{i} = 1.9$).

while the vapor phase transport should be negligible since the saturation vapor pressure is exceedingly low in this temperature range, e.g. $p_\text{sat} \sim 100\,\text{Pa}$ at $-20\,^\circ\text{C}$ and $\sim 40\,\text{Pa}$ at $-30\,^\circ\text{C}$.

It can be seen from Fig. 5 that the gap in the product water between -20 and $-30\,^\circ\text{C}$ amounts to about 0.3–0.4 mg cm^{-2} for partially dry membranes. The larger product water at $-20\,^\circ\text{C}$ is attributed mainly to the higher water diffusivity, and hence more water storage in the membrane. If the initial membrane is fully hydrated (i.e. $\Delta\lambda \to 0$), the difference in the cumulative product water diminishes between -20 and $-30\,^\circ\text{C}$ because the product water primarily accumulates in the CL pores in this situation.

3.2. Effect of current density

In Fig. 5, an additional data point shows the product water at $-30\,^\circ\text{C}$ and $80\,\text{mA cm}^{-2}$. This data point can be compared with the curve for $40\,\text{mA cm}^{-2}$ to demonstrate a strong effect of current density. The higher current density results in smaller product water, because less time is given for product water to be transported in the membrane. Consequently, the ice formation is more severe in the cathode CL at higher current densities, causing more blockage of oxygen transport and premature shutdown [11].

To further illustrate the effect of current density, two sets of cold-start experiments are compared in Fig. 6. In one set the startup current density is $100\,\text{mA cm}^{-2}$ without initial ramp; the other has the current density of $40\,\text{mA cm}^{-2}$ with initial current ramp of $0.5\,\text{mA cm}^{-2}\,\text{s}^{-1}$ for 80 s. Both experiments were conducted after dry purge at $55\,^\circ\text{C}$ for 90 s prior to cool down, and the estimated water content in the membrane was initially $\lambda_\text{i} = 1.9$ for both cases. Starting from the identical initial condition, the test with $100\,\text{mA cm}^{-2}$ current density operated for only 40 s, while the one with $40\,\text{mA cm}^{-2}$ could operate for $\sim 180\,\text{s}$. Fig. 7 plots the relation between the iR-free voltage and the cumulative product water (proportional to operational time). For the same amount of cumulative product water, perhaps $0.2\,\text{mg cm}^{-2}$, the higher current density startup already shows an onset of voltage drop, while the $40\,\text{mA cm}^{-2}$ case experiences almost no drop in voltage yet. The total product water is 0.32 and $0.51\,\text{mg cm}^{-2}$, respectively, for high and low current densities.
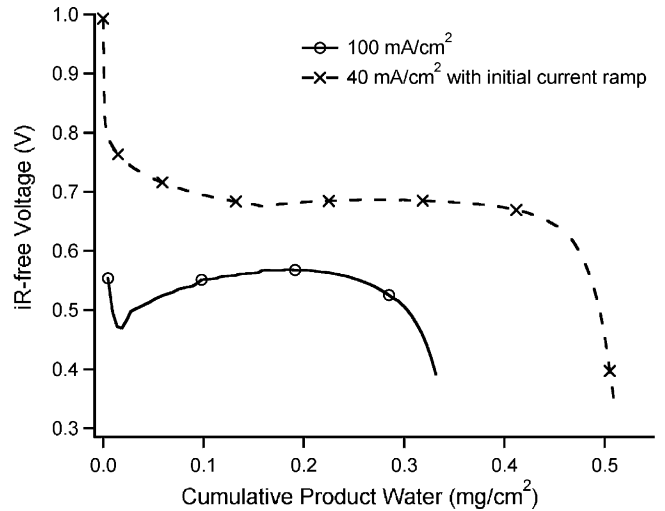
More experimental results on the current density effect under dry purge are shown in Fig. 8, along with the corresponding model predictions made earlier by Mao et al. [10]. Here the cell was operated at $-20\,^\circ\text{C}$ with current density of either $40\,\text{mA cm}^{-2}$ (with current ramp) or $100\,\text{mA cm}^{-2}$ (without current ramp) for various membrane water uptake potential $\Delta\lambda$. This figure clearly demonstrates that the low current density operation results in high product water during cold start. The computational results agree well with the experimental data.

3.3. Effects of purge duration and startup temperature after dry purge

In dry purge experiments, the initial membrane water content can be controlled by purge duration. Fig. 9 shows the time evolution of cell voltage during startup from $-20\,^\circ\text{C}$ with three different dry purge durations of 15, 30, or 60 s at a cell temperature of $55\,^\circ\text{C}$. The corresponding initial membrane water

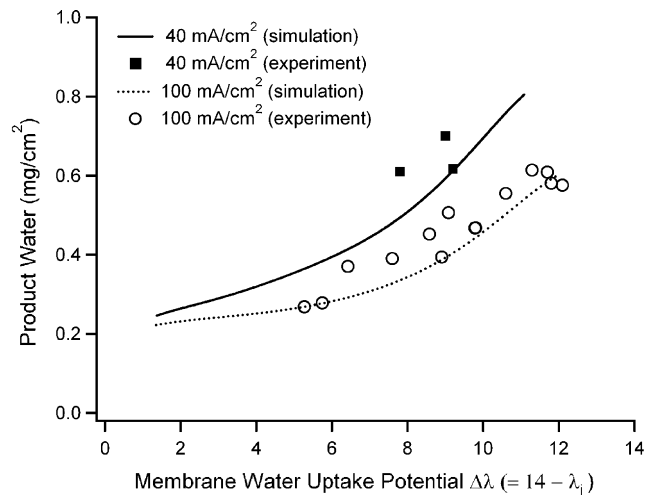Fig. 8. Relation between product water and membrane water uptake potential for the startup from $-20\,^\circ\text{C}$ under dry purge for different current densities. The simulation results are reproduced here from [10].
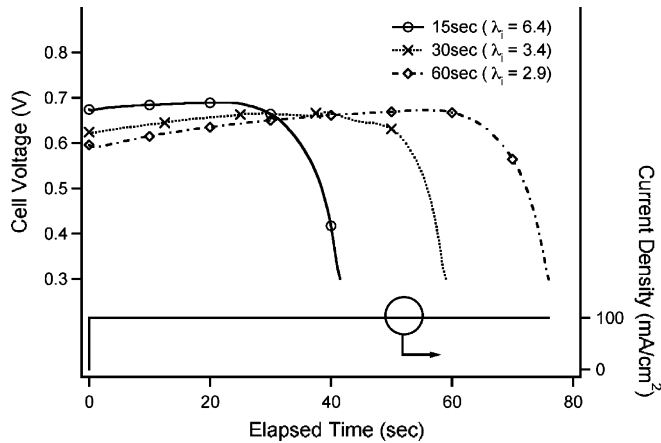
Fig. 9. Time evolution of current density and cell voltage during startup from −20 °C for different dry purge durations.

Fig. 11. Relation between product water and membrane water uptake potential for the startup from −20 and −30 °C under dry purge and 100 mA cm^{-2}.

content was $\lambda_i = 6.4$, 3.4, and 2.9, respectively. Two remarkable characteristics in the voltage curves can be seen in Fig. 9 under the current density of 100 mA cm^{-2}. First, the initial cell voltage is lower for longer purge duration that corresponds to the lower membrane water content. This is mainly because the drier membrane exhibits lower proton conductivity and therefore higher ohmic drop under the load. Secondly, the cold start operation lasts longer if the purge duration is longer. Again, this is because the drier membrane can take up more product water, and therefore the ice accumulation rate is lower within the cathode CL and cell shutdown is delayed. Another possible reason is that longer purge duration results in less residual water in the CL or more open pores.

Fig. 10 shows the dry purge cold start results from −30 °C with two different purge durations. The dry purge of 60 and 90 s at 55 °C yields membrane water content of $\lambda_i = 3.4$ and 1.9, respectively. Similar to the −20 °C startup cases shown in Fig. 9, the lower initial membrane water content gives rise to lower cell voltage. However, the operation time remains nearly the same for the two different initial water contents. The similar operation time in spite of different purge duration implies that the limiting
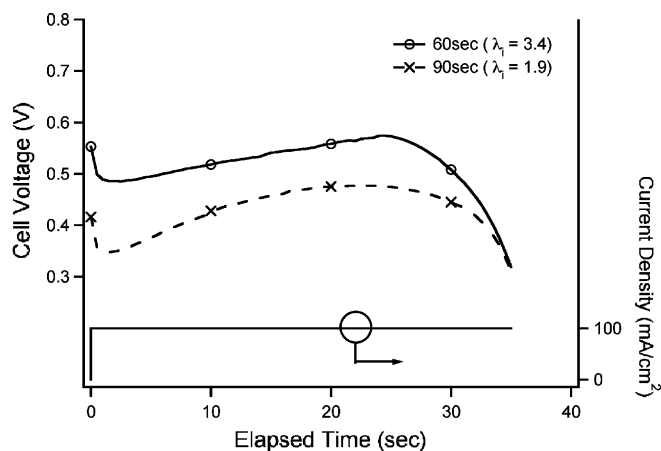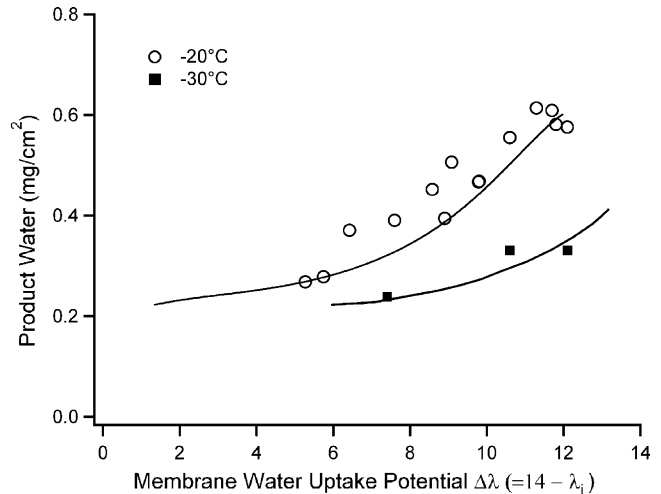
factor in the startup from −30 °C is not the membrane water uptake potential, but the residual water within the CL pores.

Fig. 11 compares the cumulative product water for cold start after dry purge for two startup temperatures, −20 and −30 °C. This map shows a similar trend to the equilibrium purge cold start displayed in Fig. 5, except for two major differences. First, the product water at the $\Delta\lambda \rightarrow 0$ limit is smaller than that after equilibrium purge. This clearly indicates existence of residual water in the cathode CL after dry purge whereas the CL is free of water after equilibrium purge. Secondly, the product water difference between −20 and −30 °C is smaller (0.15–0.3 mg cm^{-2}) than the equilibrium purge case (0.3–0.4 mg cm^{-2}) shown in Fig. 5. This can be explained by the different current densities applied in dry purge (100 mA cm^{-2}) versus equilibrium purge (40 mA cm^{-2}). Higher current density applied in the dry purge experiments diminishes the role of the membrane in storing product water and postponing the shutdown of CL by ice. Also note the two data points in the case of −30 °C for $\lambda_i = 3.4$ and 1.9; the product water is essentially the same, in consistency with Fig. 10. The same product water results from the fact that the variation in product water with a small change in initial water content (i.e. from $\lambda_i = 3.4$–1.9) is so small that it falls into the range of experimental uncertainty.

3.4. Effect of purge methods

The cold-start performance for two different purge modes are directly compared in Figs. 12 and 13 for −20 and −30 °C startup, respectively. It should be noted that two parameters differ between these two experimental sets: the purge method as well as the startup current density (see Table 1). Therefore, the difference in product water shown in Figs. 12 and 13 is contributed by both factors.

Generally, the product water is seen to increase with the membrane water uptake potential $\Delta\lambda$. Furthermore, the equilibrium purge startup has roughly 0.5 and 0.3 mg cm^{-2} higher product water than that of the dry purge startup at −20 °C (Fig. 12) and −30 °C (Fig. 13), respectively. The reasons for lower product

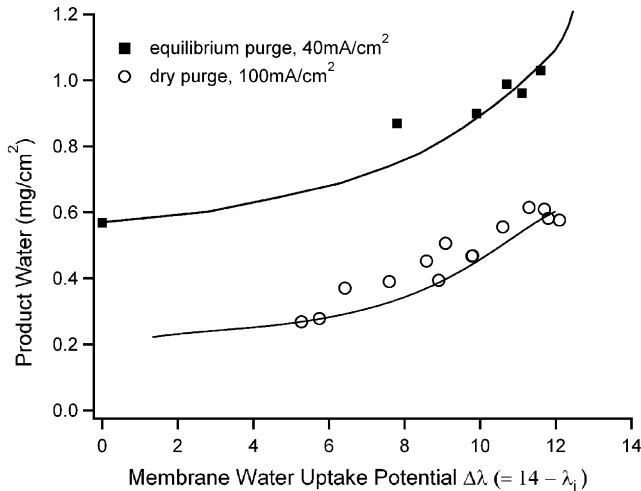Fig. 10. Time evolution of current density and cell voltage during startup from −30 °C for different dry purge durations.

Fig. 12. Relation between product water and membrane water uptake potential for the startup from −20 °C for different purge methods.

water in dry purge startup are the higher current density and the presence of residual water in the CL pores.

3.5. Effect of membrane thickness

Finally, as a major MEA design parameter, the effect of membrane thickness was examined. A membrane of double thickness (60 μm) was studied and compared with the baseline MEA based on 30 μm membrane, while keeping the other properties of the MEA the same. The equilibrium purge method was used to show the membrane thickness effect, because this mode of cold start depends more on the membrane properties. The advantage of a thick membrane is its high water storage capacity, but the disadvantages include the high membrane resistance and possibly low utilization of full water storage capacity.

As shown in Fig. 14, the experimental lines of the baseline and thicker membranes undergo a crossover at $\Delta\lambda \sim 10$. For $\Delta\lambda < 10$ the thicker membrane has smaller product water than the thinner one. However, for $\Delta\lambda > 10$ the thicker membrane results in higher product water or better cold-start performance. In other
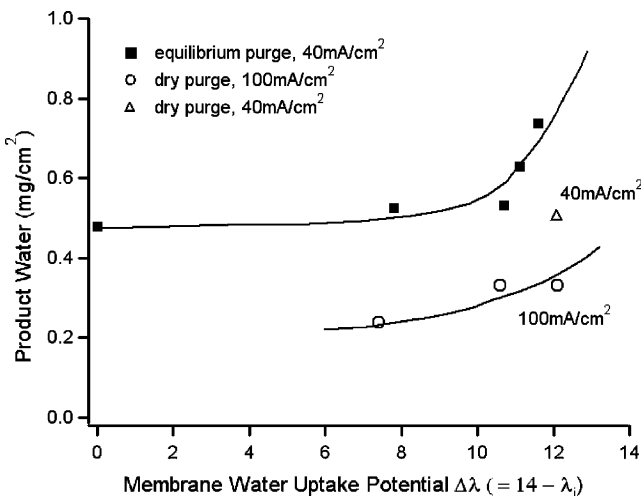

Fig. 13. Relation between product water and membrane water uptake potential for the startup from −30 °C for different purge methods.
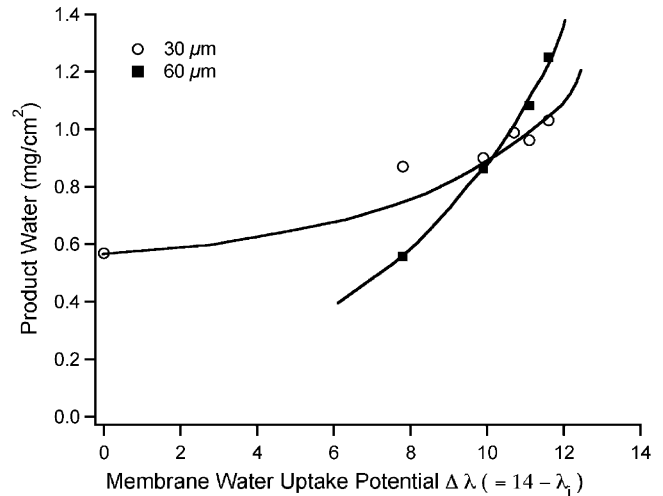

Fig. 14. Relation between product water and membrane water uptake potential for startup from −20 °C with equilibrium purge and 40 mA cm⁻² for different membrane thickness.

words, it appears that under drier initial conditions the thicker membrane is more advantageous. This experimental evidence appears to be inconsistent with a previous model prediction of Mao et al. [10] where a 30 μm membrane was compared with a 45 μm membrane, yielding negligible difference between the two. We believe that the influence of membrane thickness requires further clarification in future work.

4. Conclusions

We have investigated the effects of various operating and design parameters on PEFC cold-start performance under the isothermal boundary condition. The parameters examined here included the startup temperature, startup current density, initial membrane water content, purge duration, and membrane thickness. In addition, we compared two purge methods: equilibrium purge using partially humidified purge gas and dry gas purge. The following conclusions can be drawn from this study:

(1) The startup temperature strongly affects cold-start performance quantified by the cumulative product water. In cases of equilibrium purge, the product water increases drastically with the startup temperature, and at −3 °C the cell can operate indefinitely.

(2) The startup current density strongly impacts the product water in both equilibrium purge and dry purge. At high current density the product water becomes small, because less time is offered for the membrane to absorb and store product water.

(3) In the case of dry purge, the purge duration is a decisive operating parameter controlling the cold-start performance. As the purge duration increases, the membrane becomes drier and the residual water in the CL pores prior to cold start is reduced. As a result, the product water during cold start increases.

(4) The equilibrium purge cold start has 0.5 and 0.3 mg cm⁻² larger product water than the dry purge cold start for −20

and $-30\,^\circ$C, respectively. Diminished product water in dry purge cold start is due to the presence of the residual water in the CL pores, as well as the higher current density employed in dry purge experiments. The smaller difference in $-30\,^\circ$C startup is due to the lower water diffusivity in the membrane.

(5) The effect of membrane thickness depends on the initial membrane water content. Under drier initial conditions, a thicker membrane yields better cold-start performance.

Acknowledgement

References

[1] R.C. McDonald, C.K. Mittelsteadt, E.L. Thompson, Fuel Cells 4 (2004) 208–213.

[2] E.A. Cho, J.J. Ko, H.Y. Ha, S.A. Hong, K.Y. Lee, T.W. Lim, I.H. Oh, J. Electrochem. Soc. 150 (2003) A1667–A1670.

[3] E.A. Cho, J.J. Ko, H.Y. Ha, S.A. Hong, K.Y. Lee, T.W. Lim, I.H. Oh, J. Electrochem. Soc. 151 (2004) A661–A665.

[4] F. Kagami, T. Ogawa, Y. Hishinuma, T. Chikahisa, Simulating the performance of a PEFC at a temperature below freezing in Fuel Cell Seminar Abstract, 2002.

[5] Y. Hishinuma, T. Chikashisa, F. Kagami, T. Ogawa, JSME Int. J. B 47 (2004) 235–241.

[6] M. Oszcipok, D. Riemann, U. Kronenwett, M. Kreideweis, M. Zedda, J. Power Sources 145 (2005) 407–415.

[7] M. Oszcipok, M. Zedda, D. Riemann, D. Geckeler, J. Power Sources 154 (2006) 404–411.

[8] S. Ge, C.Y. Wang, Electrochem. Solid-State Lett. 9 (2006) 499–503.

[9] L. Mao, C.Y. Wang, J. Electrochem. Soc. 154 (2007) B139–B146.

[10] L. Mao, C.Y. Wang, Y. Tabuchi, J. Electrochem. Soc., in press.

[11] K. Tajiri, Y. Tabuchi, C.Y. Wang, J. Electrochem. Soc. 154 (2007) B147–B152.

[12] T.E. Springer, T.A. Zawodzinski, S. Gottesfeld, J. Electrochem. Soc. 138 (1991) 2334–2342.